Electronic Supplementary Material (ESI) for Physical Chemistry Chemical Physics.
This journal is © the Owner Societies 2015

Supplementary Information

Evaluation of Intrinsic Charge Carrier Transporting Properties of Linear- and Bent- Shaped π-Extended Benzo-Fused Thieno[3,2-b]thiophenes

Yusuke Tsutsui, Tsuneaki Sakurai,* Sojiro Minami, Koji Hirano, Tetsuya Satoh, Wakana Matsuda, Kenichi Kato, Masaki Takata, Masahiro Miura* and Shu Seki*

Department of Applied Chemistry, Graduate School of Engineering, Osaka University, 2-1 Yamadaoka, Suita, Osaka 565-0871, Japan.

RIKEN SPring-8 Center, 1-1-1 Kouto, Sayo-cho, Sayo-gun, Hyogo 679-5148, Japan

*Correspondence and requests for materials should be addressed to Tsuneaki Sakurai (t-sakurai@chem.eng.osaka-u.ac.jp), Masahiro Miura (miura@chem.eng.osaka-u.ac.jp), and Shu Seki (seki@chem.eng.osaka-u.ac.jp).

1. Methods

Electronic absorption spectra were recorded on a JASCO model V-570 spectrometer. Fluorescence spectra were recorded on a Hitachi High-Technologies Co. model F-2700 spectrometer. Tapping-mode atomic force microscopy (AFM) was performed on a SII NanoTechnology model Nanonavi II with silicon cantilevers (OMCL-AC200TS-R3, OLYMPUS). The HOMO energy levels were estimated by UV photoelectron yield spectroscopy (PYS) using a Sumitomo Heavy Industry model PCR-102 spectrometer, where the photon energy was adjusted from 4.0 to 8.0 eV with an interval of 0.1 eV. Thin film samples were prepared by vapor deposition on an ITO-coated glass plate and loaded into a vacuum chamber, evacuated at ca. 5×10^{-4} Pa. A deuterium lamp was used as an excitation source, where the anode voltage was fixed at 10 V. The threshold photon energy was estimated from the photoelectron yield spectrum. DFT calculations were carried out using B3LYP functional and the basis set 6-31G(d) by Gaussian 09 program package (Revision A.02).[S1] Structure optimizations and energy calculations of BBTBDT and *iso*-BBTBDT were performed under designated point groups C_{2h}, and C_{2v}, respectively. Calculated vibration modes resulted in no imaginary frequency and same structures were obtained without specific symmetries representing the most stable structures of both compounds. Powder X-ray diffraction (XRD) measurements were carried out using a synchrotron radiation X-ray beam with a wavelength of 1.08 Å on BL44B2 at the Super Photon Ring (SPring-8, Hyogo, Japan). A large Debye-Scherrer camera was used in conjunction with an imaging plate as a detector, and all diffraction patterns were recorded with a 0.01 ° step in 2θ. During the measurements, samples were put into a 0.5-mm thick glass capillary and rotated to obtain a homogeneous diffraction pattern. The exposure time to the X-ray beam was 3 min, where samples were prepared by cooling their isotropic melts at a rate of 10 °C min^{-1} and annealed for 2 min. XRD measurements of powders or vapor-deposited films on a quartz plate were performed on a Rigaku model MiniFlex600 X-ray diffractometer equipped with a X-ray tube using Cu Kα radiation beam with a wavelength of 1.54 Å. Diffraction intensities were recorded with a 0.02 ° step in 2θ. Flash-photolysis time-resolved microwave conductivity (FP-TRMC) measurements were carried out under ambient atmosphere at room temperature, where the resonant frequency and microwave power were properly adjusted at 9.1 GHz and 3 mW, respectively. Charge carriers were photochemically generated using a third harmonic generation (λ = 355 nm) of a Spectra Physics model INDI-HG Nd:YAG laser with a pulse duration of 5–8 ns. The photon density of the 355 nm laser pulse was 4.6×10^{15} photons cm^{-2}

pulse^{-1}. The TRMC signal picked up by a diode (rise time < 1 ns) was monitored by a Tektronix model TDS 3032B digital oscilloscope. The observed conductivities, given by a photocarrier generation yield (ϕ) multiplied by the sum of charge carrier mobilities ($\Sigma\mu$), were normalized according to the equation; $\phi\Sigma\mu = (1/eAI_0F_{\mathrm{light}})(\Delta P_{\mathrm{r}}/P_{\mathrm{r}})$, where, e, A, I_0, F_{light}, P_{r}, and ΔP_{r} represent unit charge of a single electron, sensitivity factor (S^{-1} cm), incident photon density of the excitation laser (photon cm^{-2}), correction (or filling) factor (cm^{-1}), and reflected microwave power and its change, respectively. The samples for FP-TRMC measurement were fabricated in a powder form or vapor-deposited film. The former was prepared by putting the powder onto a quartz plate with a double-sided sticky tape. The latter was prepared by vapor-deposition of a ca. 30–180 nm thick organic semiconducting layer onto a quartz plate at a rate of 0.3–0.5 Å s^{-1} in thickness. Field-induced time-resolved microwave conductivity (FI-TRMC) measurements were performed with a microwave circuit using X-band microwaves under ambient atmosphere at room temperature. The microwave frequency was adjusted to 9.0 GHz by using a Rohde Schwarz model SMF 100A signal generator. After a metal–insulator–semiconductor (MIS) device was set in the microwave cavity, a 50-ms pulse gate bias voltage V_{g} was applied using a Wave Factory model WF 1973 multifunction generator, where the change of the reflected microwave power (ΔP_{r}) and the current injected into the semiconductor–insulator interface (I_{inj}) were measured using a Tektronix model TDS 3052B digital phosphor oscilloscope. The MIS devices for FI-TRMC measurement were fabricated by the following procedure and all quartz substrates for devices were treated with UV/O_3 prior to use. 5 nm Ti as an adhesion layer and 20 nm bottom Au electrode were deposited onto a quartz substrate by DC sputtering with Ar and vapor deposition under vacuum condition at around 4×10^{-1} and 4×10^{-4} Pa, respectively. On top of them, 250 nm SiO_2 were sputtered by 100 W RF sputtering. A PMMA layer was fabricated by spin-coating of its 3 wt% toluene solution at 2000 rpm for 30 s, followed by the annealing at 180 °C for 1 h. Then, ca. 30 nm-thick organic semiconducting layer was vapor-deposited at a rate of 0.3–1.0 Å s^{-1} in thickness onto the PMMA layer in an evaporated chamber, evacuated at ca. 4×10^{-4} Pa. Finally, a 20 nm-thick top Au electrode was vapor-deposited on top of the semiconducting layer.

2. Supporting Figures and Tables

BBTBDT			*iso*-BBTBDT		
2θ / °	*d* / Å	*hkl*	2θ / °	*d* / Å	*hkl*
3.51	17.63	100	3.60	17.19	100
7.02	8.83	200	4.03	15.36	1’00
10.67	5.81	300	8.08	7.66	2’00
14.47	4.29	400	8.77	7.06	
16.60	3.74	500	8.99	6.89	
18.98	3.28		18.11	3.43	
19.16	3.24		18.57	3.35	

C8-BBTBDT			C8-*iso*-BBTBDT		
2θ / °	*d* / Å	*hkl*	2θ / °	*d* / Å	*hkl*
1.76	35.16	100	1.70	36.40	100
2.66	23.27		2.25	27.50	
3.52	17.58	200	2.92	21.19	
7.04	8.80	400	3.73	16.59	
8.79	7.03	500	12.94	4.79	
10.58	5.86	600	13.08	4.66	
13.05	4.75		15.57	3.99	
13.15	4.72		17.95	3.46	
15.75	3.94		18.69	3.33	
18.92	3.29				

C8-BBTBDT from ODCB solution		
2θ / °	*d* / Å	*hkl*
1.74	35.36	100
2.65	23.35	1’00
3.50	17.68	200
5.32	11.64	2’00
7.03	8.81	400
9.42	6.58	
14.07	4.41	
17.02	3.65	

Table S1. List of obvious diffraction peaks from their observed XRD patterns with their *d*-spacing value and *hkl* index.

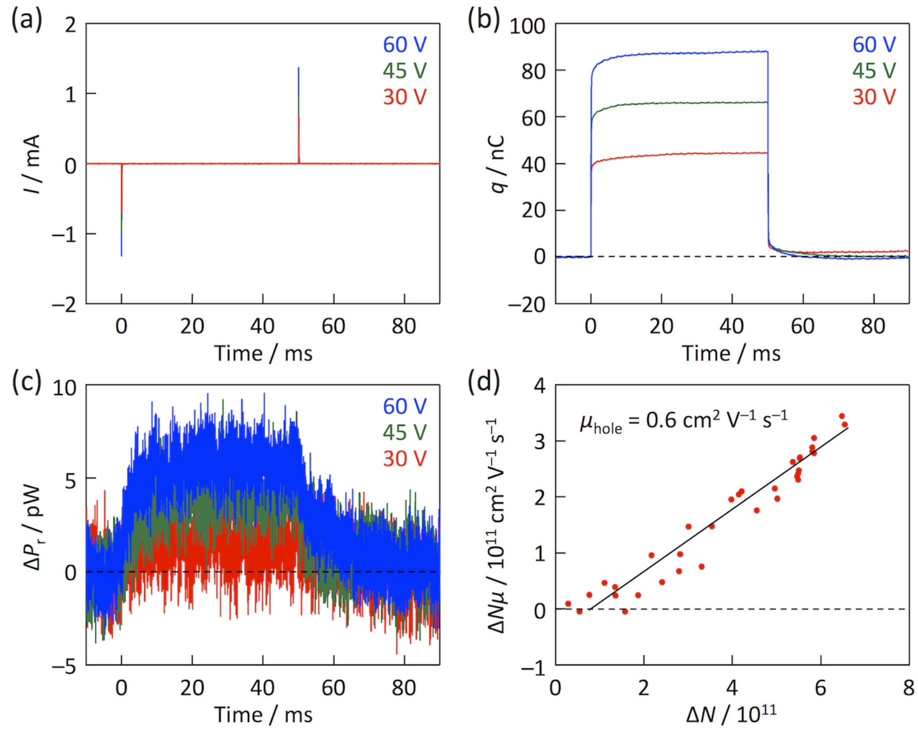

Fig. S2. (a) Typical kinetic profiles of current flow injected into an *iso*-BBTBDT-based MIS device under application of negative gate bias. (b) Typical charge amount profiles calculated from (a). (c) Typical Kinetic profiles of changes in reflected microwave power under application of negative bias. (d) ΔN–$\Delta N\mu$ plot. ΔN was evaluated from saturated values of q while $\Delta N\mu$ was calculated from ΔP_r.

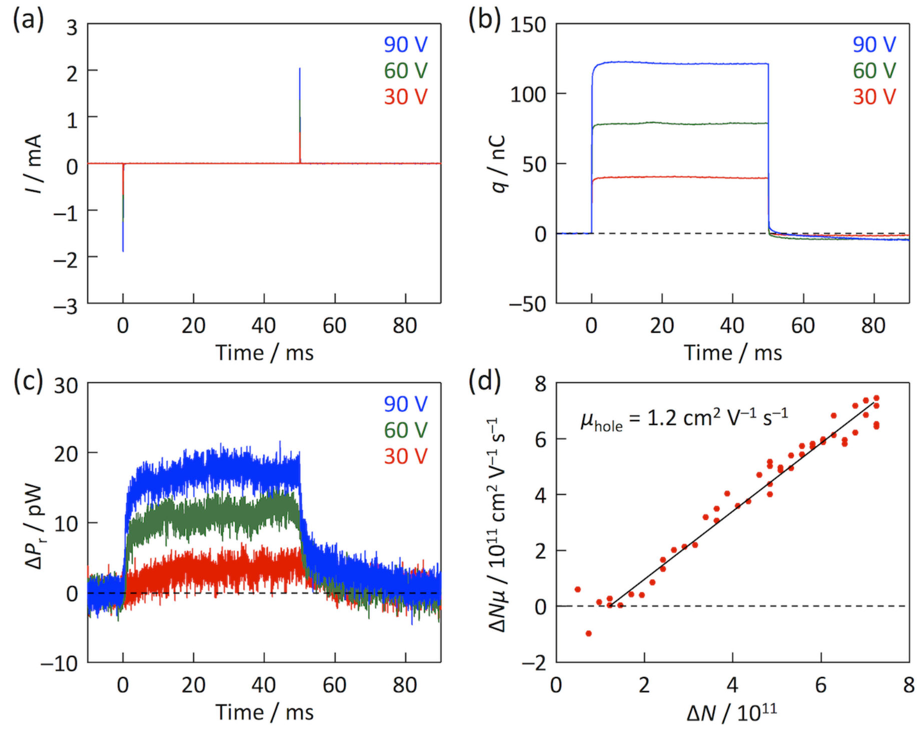

Fig. S3. (a) Typical kinetic profiles of current flow injected into a C8-BBTBDT-based MIS device under application of negative gate bias. (b) Typical charge amount profiles calculated from (a). (c) Typical Kinetic profiles of changes in reflected microwave power under application of negative bias. (d) ΔN–$\Delta N\mu$ plot. ΔN was evaluated from saturated values of q while $\Delta N\mu$ was calculated from ΔP_r.

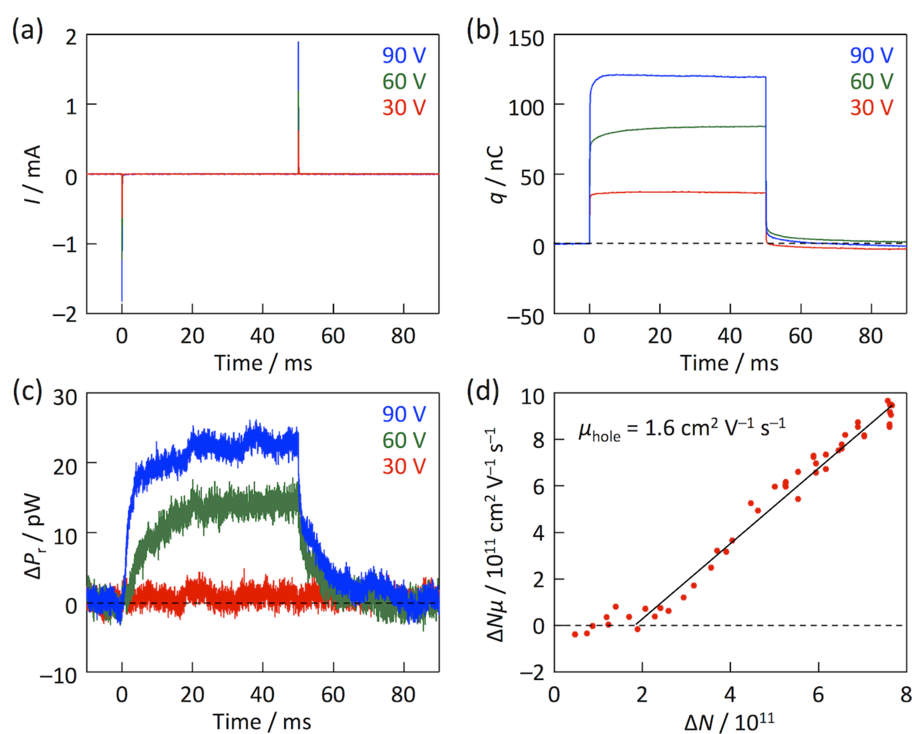

Fig. S4. (a) Typical kinetic profiles of current flow injected into a C8-*iso*-BBTBDT-based MIS device under application of negative gate bias. (b) Typical charge amount profiles calculated from (a). (c) Typical Kinetic profiles of changes in reflected microwave power under application of negative bias. (d) ΔN–$\Delta N\mu$ plot. ΔN was evaluated from saturated values of q while $\Delta N\mu$ was calculated from ΔP_r.

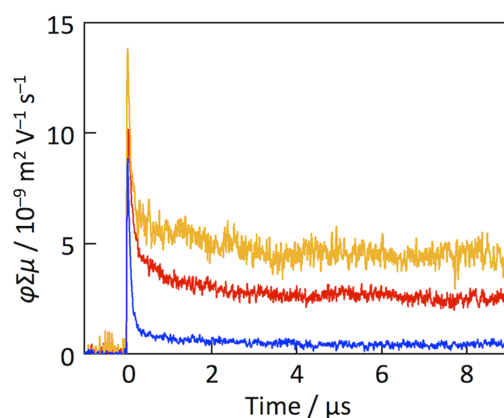

Fig. S5. Kinetic traces of transient conductivity observed for vapor-deposited films of BBTBDT (red), *iso*-BBTBDT (blue) and C8-BBTBDT (yellow).

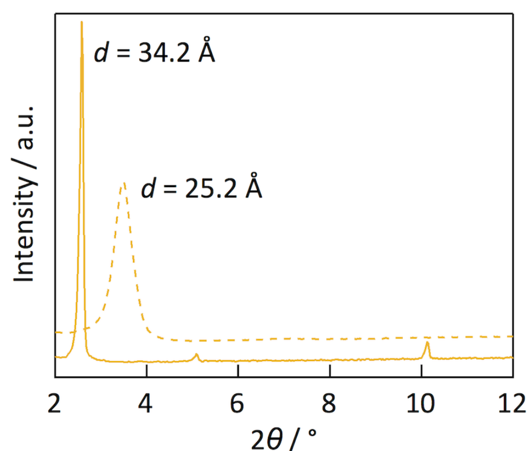

Fig. S6. X-ray diffraction patterns of C8-BBTBDT in the powder form (solid line) and thin film (dashed line). The *d* spacing value of the powder is consistent with synchrotron XRD measurements. See Figure 2b and Table S1.

3. Supporting References

(S1) Gaussian 09, Revision A.02, M. J. Frisch, G. W. Trucks, H. B. Schlegel, G. E. Scuseria, M. A. Robb, J. R. Cheeseman, G. Scalmani, V. Barone, B. Mennucci, G. A. Petersson, H. Nakatsuji, M. Caricato, X. Li, H. P. Hratchian, A. F. Izmaylov, J. Bloino, G. Zheng, J. L. Sonnenberg, M. Hada, M. Ehara, K. Toyota, R. Fukuda, J. Hasegawa, M. Ishida, T. Nakajima, Y. Honda, O. Kitao, H. Nakai, T. Vreven, J. A. Montgomery, Jr., J. E. Peralta, F. Ogliaro, M. Bearpark, J. J. Heyd, E. Brothers, K. N. Kudin, V. N. Staroverov, R. Kobayashi, J. Normand, K. Raghavachari, A. Rendell, J. C. Burant, S. S. Iyengar, J. Tomasi, M. Cossi, N. Rega, J. M. Millam, M. Klene, J. E. Knox, J. B. Cross, V. Bakken, C. Adamo, J. Jaramillo, R. Gomperts, R. E. Stratmann, O. Yazyev, A. J. Austin, R. Cammi, C. Pomelli, J. W. Ochterski, R. L. Martin, K. Morokuma, V. G. Zakrzewski, G. A. Voth, P. Salvador, J. J. Dannenberg, S. Dapprich, A. D. Daniels, O. Farkas, J. B. Foresman, J. V. Ortiz, J. Cioslowski, and D. J. Fox, Gaussian, Inc., Wallingford CT, 2009.